https://doi.org/10.17221/101/2025-RAE

Modelling the hydration process of wheat grain with layer-dependent diffusion coefficients

Bakhtiyar Ismailov[1,2], *Abdushukur Urinboev*[2]*, *Khairulla Ismailov*[1], *Akmaljon Kuchkarov*[2]

[1]*Department of Information Systems and Modelling, Faculty of Information Technologies and Energy, M. Auezov South Kazakhstan University, Shymkent, Kazakhstan*
[2]*Department of Electronics and Instrumentation, Faculty of Energy Engineering and Technology, Fergana State Technical University, Fergana, Uzbekistan*

**Corresponding author: urinboevabdushukur@gmail.com*

Citation: Ismailov B., Urinboev A., Ismailov Kh., Kuchkarov A. (2026): Modelling the hydration process of wheat grain with layer-dependent diffusion coefficients. Res. Agr. Eng., 72: 25–40.

Abstract: This study develops and validates a multilayer diffusion model of wheat grain hydration that incorporates layer-dependent diffusion coefficients for bran, endosperm, and germ. The moisture transport is formulated using Fick's law with two interface formulations: (*i*) classical continuity of the concentration and flux and (*ii*) an interlayer resistance formulation that permits concentration discontinuities. Diffusion coefficients and geometric parameters were determined experimentally; A 3D grain model (structured-light scanning, COMSOL Multiphysics) informed the computational domain. Numerical solutions combined eigenfunction expansions with finite-difference discretisation near the interfaces. Across eight winter wheat varieties, the diffusion coefficients spanned 11.6 – 20.5 × 10^{-12} $m^2 \cdot s^{-1}$ (mean 16.27 ± 3.08 × 10^{-12} $m^2 \cdot s^{-1}$). Relative to the continuity model, the resistance model reduced the early-stage endosperm over-prediction by ~ 0.6–1.0 % (absolute) and lowered the whole-grain RMSE by ~ 20–30% over 0–240 min. These results support the role of thin moisture-retaining films as active barriers and yield smooth, real-time-ready outputs suitable for the automated control of pre-milling hydration; the framework is extensible to full 3D transient simulations.

Keywords: grain hydration; interlayer resistance; multilayer model; moisture transport; COMSOL Multiphysics; modelling; micropyle

The primary stages involved in preparing wheat grain for milling include grain reception, cleaning, hydration, threshing, and sifting. Among these processes, hydration plays a crucial role in ensuring consistent flour quality and energy-efficient grinding. Modern milling enterprises are increasingly implementing automated process control systems (APCSs) and digital analytical methods, including the mathematical modelling of moisture transport.

Although many studies address wheat hydration, most focus only on the morphological changes or provide empirical descriptions of water absorption. For instance, Zhou et al. (2023) describe a grain model using tomography and discrete modelling methods, providing an overview of the physical and mechanical properties. Using digital image processing (SmartGrain), the morphology of 120 wheat varieties before and after hydration was analysed, but the physicochemical nature of the process, including the diffusion coefficients and resistance to interlayer moisture exchange was not considered. In the study by Barrer et al. (2019), the phases of water absorption and shape changes over time were described, yet no quan-

https://doi.org/10.17221/101/2025-RAE

titative analysis of the internal moisture transfer within the grain structure was provided. Additionally, the calculations and modelling of the modulus of elasticity were considered, which are useful for understanding diffusion resistances in grain layers. Jia et al. (2015) evaluated diffusion coefficients for different grain sections, but employed simplified geometric assumptions (spherical or ellipsoidal shapes) without considering the real morphology. Some studies, including Voicu et al. (2013), have evaluated the grain elasticity and mechanical characteristics, but have rarely accounted for the layered structure and gradient diffusion coefficients. Research on the post-harvest processing and thermal impacts on the grain moisture content and properties emphasises the importance of a comprehensive approach to moisture exchange modelling (Steidle et al. 2015; Müller et al. 2022; Liu et al. 2023; Kang et al. 2024; Yigit et al. 2024). Studies on the spatial grain morphology using 3D modelling and shape analysis directly relate to the geometric module of our model (Huang et al. 2022; Anders 2023). Algorithms for digital moisture forecasting using artificial intelligence and parametric modelling have been described (Singh and Heldman 2009; Cao et al. 2024). The concepts of interlayer diffusion resistance and mass transfer have been substantiated (Ismailov et al. 2013, 2021), highlighting the necessity of considering the grain anatomical structure and biochemical characteristics, as noted by Khalid et al. (2023). Additionally, Dimech et al. (2024) modelled the moisture exchange in multilayer systems, while Khan et al. (2024) and Bharathi et al. (2023) provided data on the moisture distribution and accumulation, reinforcing the importance of the initial moisture and grain geometry. The theoretical foundation of our model is based on the classical diffusion theory as presented by Mazumdar (1999). Furthermore, the subdivision of the interaction domain into multi-connected regions has previously been applied to problems with high velocities and periodic boundary conditions by Vlasák et al. (2005).

However, the existing studies do not adequately account for the layered structure of wheat grain (bran, aleurone layer, endosperm) and do not model the interlayer diffusion resistance, especially critical during the initial hydration stages. Moreover, no integrated approach combining a grain morphology analysis and the physical-mathematical modelling of the moisture diffusion in heterogeneous media has been proposed. Recent studies on water movement in mature wheat grains (*Triticum aestivum* L.), both dormant and non-dormant genotypes, using magnetic resonance micro-imaging (MRMI) (Rathjen et al. 2009), have demonstrated that water penetrates the micropyle channel during the earliest stages of hydration. After just 2 h, water was clearly visible in the micropyle, and after 12 h the germ structures (coleoptile and radicle) were distinctly differentiated. This finding confirms the necessity of considering the heterogeneity of grain layers and their diffusion coefficients when modelling water penetration processes in wheat grain (hydration during germination and hydration in milling technology).

A recent μCT-based morphometric analysis of developing wheat grains (Le et al. 2019) together with correlation studies on the white and whole wheat flour quality (Li et al. 2023) highlights that the grain microstructure and bran distribution strongly influence the hydration behaviour, dough rheology, and final product performance.

Wheat varieties exhibit considerable variability in geometry, moisture absorption, and layer structures, necessitating adaptive models that consider spatial heterogeneity, geometry, and external condition impacts on diffusion coefficients. The present study introduces a new approach that integrates experimental and numerical methods. The radial diffusion coefficients were represented as piecewice-constant functions corresponding to the main anatomical layers (bran, endosperm, and germ). Layer-dependent diffusion coefficients were established based on a microscopic analysis and geometric measurements. Particular attention was paid to physical processes at the interlayer boundaries: capillary and adhesion effects create additional barriers to water transfer, leading to abrupt changes in the concentration gradients. These interface layers with increased resistance were formalised through modified boundary conditions, enabling the more accurate reproduction of real moisture transfer conditions. Verification of the proposed model was performed by comparing the calculated and experimental moisture distribution across layers. Structured-light scanning and microscopy provided point cloud data for constructing a 3D grain model in COMSOL Multiphysics. This model enabled the automated

https://doi.org/10.17221/101/2025-RAE

extraction of the geometric parameters. The data were integrated into the computational scheme and ultimately targeted for APCS integration to improve the responsiveness and accuracy in the hydration control of flour milling.

Therefore, the aim of this study is to develop and validate a multilayer moisture-diffusion model for wheat grain that explicitly accounts for its anatomical heterogeneity and layer-dependent diffusion coefficients. Unlike classical continuity models, the proposed approach incorporates interlayer resistance to represent the interlayer moisture-retaining films and capillary barriers at the anatomical interfaces. The geometric and diffusion parameters were determined experimentally, and a three-dimensional grain model constructed using structured-light scanning and COMSOL Multiphysics provided the input for the computational domain. Two variants of the model, with and without interfacial resistance, were implemented and quantitatively compared against time-resolved hydration measurements. The novelty of this work lies in combining a digital morphometric analysis with numerical modelling based on Fick's law, introducing gradient diffusion coefficients across the grain layers, and formalising the interlayer resistance. The model advances the predictive accuracy for moisture transfer in wheat grain and supports its integration into automated control systems for pre-milling hydration.

MATERIAL AND METHODS

The wheat grain variety Alekseevich, grown in Uzbekistan, was selected as the object of the study, due to its stable geometric parameters and widespread use in the regional milling industry. The grain's average dimensions were as follows: length of 5.6 mm, width of 2.6 mm, and thickness of 1.6 mm. In the study, data from additional wheat varieties were used to determine the range of the geometric and diffusion parameters.

Experimental determination of the geometric and diffusion parameters. Figure 1 shows the schematic anatomical structure of wheat grain, corresponding to the model adopted in Food and Agriculture Organization (FAO) methodological materials (Botany of the Wheat Plant).

This schematic illustrates the main morphological elements of the grain, including the bran, aleurone layer, endosperm, scutellum, coleoptile, germ, micropyle, and brush. This structural representation is used in the present work as the baseline model for the experimental determination of the geometric parameters and the subsequent assignment of the boundary conditions in the moisture diffusion calculations.

The experimental data for the wheat variety Alekseevich were obtained. Geometric parameters of the grain layers were measured using an AS ONE SL-700-LED Biological Microscope (up to 1 000× magnification) (AS ONE Corporation, Osaka, Japan) and INSIZE 150 digital callipers (INSIZE Co., Ltd., Suzhou, China) (accuracy: 0.01 mm). The thickness of the bran, endosperm, and germ were determined from the transverse grain sections at 20-min intervals post-hydration initiation. The gravimetric methodology was employed to ascertain the moisture diffusion coefficient within each grain layer: 100 g of dry grain were immersed in distilled water for 3 s, then removed, blotted dry, weighed, and stored in a sealed container with a humid atmosphere at 25 ± 1 °C. The mass and moisture content measurements occurred every 40 min over 12 hours. Figure 2 illustrates the microstructural features of the endosperm during the early hydration of the Alekseevich variety.

Figure 2A shows an image of the endosperm, where the first signs of swelling under hydration are

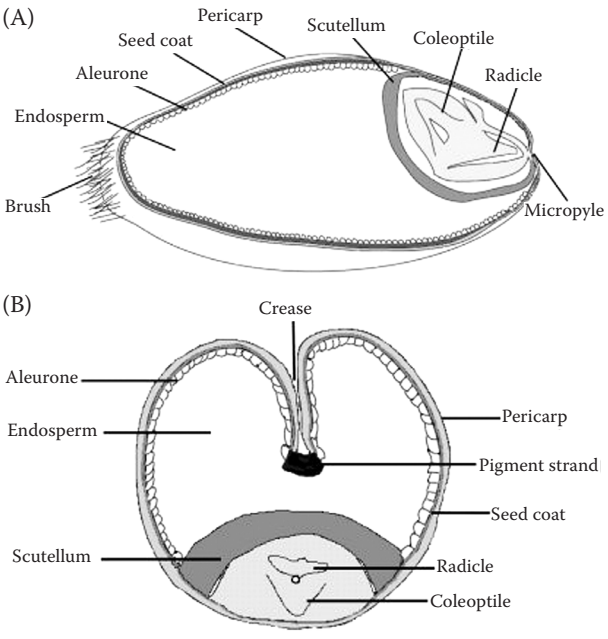

Figure 1. Schematic representation of wheat grain: (A) longitudinal section and (B) cross-section in the crease region

https://doi.org/10.17221/101/2025-RAE

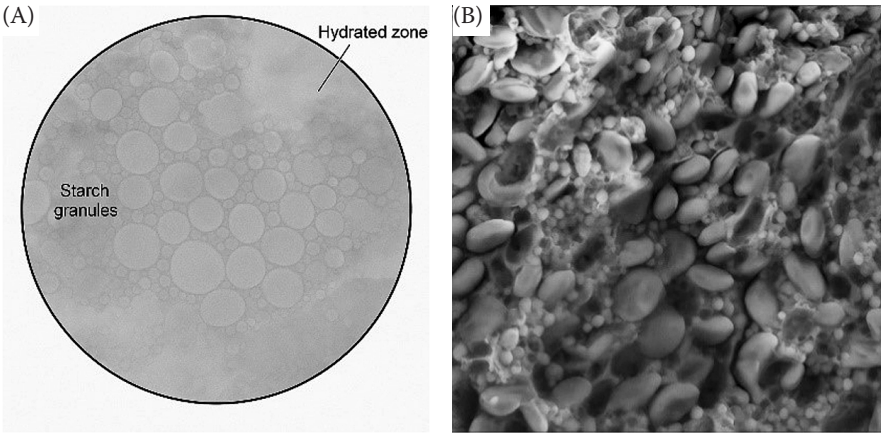

Figure 2. Micrographs of the wheat endosperm obtained by scanning electron microscopy: (A) with a 40× objective lens and (B) with a 100× objective lens

already visible. Figure 2B scanning electron microscopy (SEM) presents the morphology of the starch granules and cell walls. The three-dimensional point cloud data of wheat grains were obtained via structured light scanning methods. Figure 3 shows the morphological structure of the wheat grain.

Figure 3A shows a schematic longitudinal section with the bran and endosperm marked. Figure 3B displays a three-dimensional grain model highlighting the ventral groove, which serves as an important reference for the segmentation and morphometric analysis. Figure 3C illustrates the internal grain structure in a volumetric reconstruction, enabling assessment of the spatial distribution of tissues and their relative arrangement.

3D modelling of the grain. To refine the geometric characteristics of the wheat grain and its layers, a three-dimensional model was constructed using the COMSOL Multiphysics software package (Ver. 5.6, 2023). This visualisation helped to refine the layer boundaries and define realistic dimensions for the numerical implementation of the model. The resulting mesh was then used in discretising the diffusion problem. For the analysis of the moisture distribution within the grain, several critical factors were taken into account: identification of the coordinates for the moisture concentration measurement points, hydration duration, grain moisture concentration at various intervals, and supplementary data aiding the result interpretation. During the experiments, 200 g of distilled water were added to 100 g of wheat grain.

The model enabled the evaluation of the layer volume ratios, internal grain contours, and actual hydration points. Figure 4 presents the external surface mesh and an internal section reflecting the boundaries of the diffusion zones; this mesh was used for the spatial discretisation in the numerical calculations.

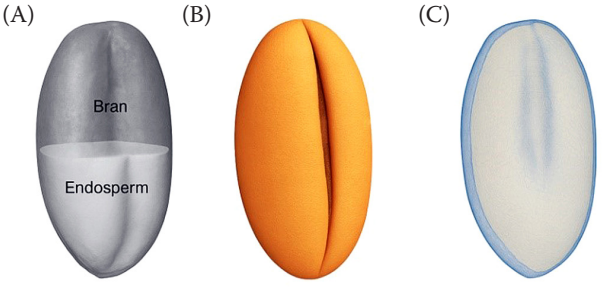

Figure 3. Morphological structure of the wheat grain: (A) longitudinal section highlighting the bran and endosperm, (B) three-dimensional grain model indicating the ventral groove, and (C) volumetric reconstruction of the internal structure

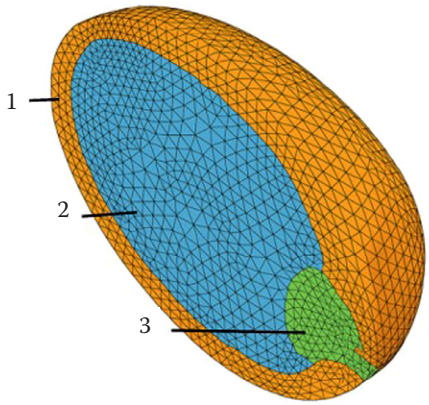

Figure 4. 3D view of the wheat grain of the Alekseevich variety
1 – bran; 2 – endosperm; 3 – germ

https://doi.org/10.17221/101/2025-RAE

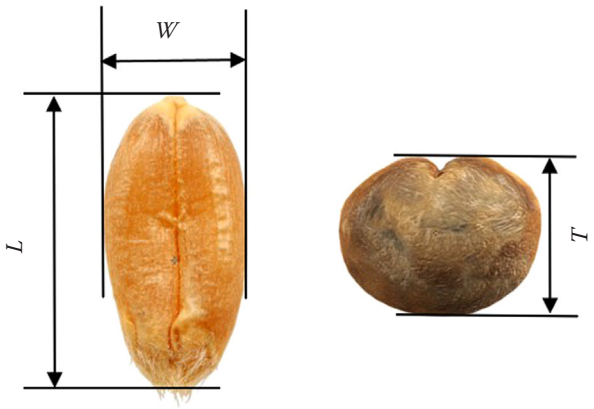

Figure 5. Main dimensions of the wheat grain
L – length (mm); W – width (mm); T – thickness (mm)

Figure 5 shows the main linear dimensions of the wheat grain of the Alekseevich variety, determined using an accuracy of ± 0.01 mm.

The following measurement ranges were obtained: length L = 4.0–7.0 mm; width W = 1.0 to 3.8 mm; and thickness T = 1.0–3.1 mm.

The geometric parameters shown in Figure 5 are used as the initial input data for implementing the mathematical model of the water diffusion in the wheat grain. To expand the applicability of the mathematical model, morphometric parameters were measured for eight of the most common winter wheat varieties grown in Uzbekistan. Table 1 presents the values of the thickness, width, length, endosperm fraction, as well as the diffusion coefficients used for the model calibration.

Experimental evaluation of the hydration dynamics. The temporal dynamics of water absorption were investigated according to the methodology described in Khalid et al. (2023). One hundred grams of dry wheat grain were immersed in 200 g of distilled water, and weighing was conducted every 40 minutes. The resulting hydration curve showed saturation up to 18.0% within 40 min, followed by a gradual desorptive decrease to an equilibrium level of approximately 16.5% over 11 hours. These results confirm a two-phase hydration mechanism: rapid initial absorption at the surface, followed by slower moisture redistribution driven by internal diffusion.

Mathematical model of the radial moisture diffusion in the wheat grain

To predict the dynamics of the moisture accumulation in the heterogeneous grain matrix, a radial diffusion model was developed based on Fick's second law. This section presents the theoretical formulation of the problem and the numerical implementation of the model describing the moisture transfer through the bran, endosperm, and germ of the wheat grain.

Problem statement. Due to the layered structure of wheat grain (bran, endosperm, germ), and the practical impermeability of the bran, together with the special structure of the micropyle (Olver et al. 2010), moisture, during the initial stage, penetrates mainly in the longitudinal direction, and then radially (radial diffusion). Thus, in strict formulation, the modelling problem is non-stationary and three-dimensional (three spatial coordinates plus time). However, as a first approximation, the problem is reduced to an axisymmetric form: the water concentration C is treated as a function of the radial coordinate r and time t. The resistance to moisture transfer varies among the layers, ne-

Table 1. Geometric characteristics and diffusion coefficients of the wheat grain for different varieties

No.	Variety	T	W	L	Endosperm (%)	D (10^{-12} $m^2 \cdot s^{-1}$)
		(mm)				
1	Bezostaya-100	1.04	1.40	4.54	77.6	17.3
2	Akhmad	1.09	1.42	4.63	80.1	16.1
3	Alekseevich	1.31	1.64	4.87	81.2	11.6
4	Gurt	1.02	1.32	4.32	76.8	18.6
5	Valena	1.07	1.43	4.56	79.4	16.4
6	Antonina	1.03	1.37	5.02	77.5	17.7
7	Grom	1.28	1.63	4.48	81.1	12.0
8	Videya	1.01	1.21	4.35	76.4	20.5

L – length; W – width; T – thickness; D – diffusion coefficient

https://doi.org/10.17221/101/2025-RAE

cessitating a modelling approach with a spatially variable diffusion coefficient. The model is based on Fick's second law, adapted for radial symmetry in spherical coordinates, as shown in Equation (1):

$$\frac{\partial C(r,t)}{\partial t} = \frac{1}{r^2}\frac{\partial}{\partial r}\left(D(r) \times r^2 \times \frac{\partial C(r,t)}{\partial r} \right) \quad (1)$$

where: $C(r,t)$ – the moisture concentration at radius r and time t; $D(r)$ – the spatially variable diffusion coefficient dependent on the radial position; r – the current radial position within the interval $(0,R)$; R – the grain radius at longitudinal section l.

The grain radius for each section along the grain length is a variable quantity $0 \le R_1 \le W/2$, where W is the grain width (Figure 5).

Initial and boundary conditions. The initial condition is given by Equation (2):

$$C(r,0) = C_0 \quad (2)$$

where: C_0 – the moisture concentration of the grain at the beginning of milling.

The boundary condition on the grain surface is defined by Equation (3):

$$C(R,t) = C_s \quad (3)$$

where: C_s – the surface water concentration, which remains close to unity throughout the process (the grain is fully immersed in a moist medium).

Impermeability at the bran layer is represented by Equation (4):

$$\frac{\partial C}{\partial r}|_{r=R_1} = 0 \quad (4)$$

The symmetry condition along the grain axis, from the micropyle to the brush, is represented by Equation (5):

$$\frac{\partial C}{\partial r}|_{r=0} = 0 \quad (5)$$

The micropyle condition describing rapid water penetration at the initial stage (Rathjen et al. 2009) is expressed by Equation (6):

$$C(l=0,r=0,t) = C_s,\ \frac{\partial C}{\partial l}|_{l=0} = D_{mp},\ 0 \le t \le T_1 \quad (6)$$

Table 2. Radial layer structure and diffusion coefficients in the wheat grain model

Layer	Radial position (r)	Diffusion coefficient $D(r)$
Bran	$0.8R < r \le R$	D_1
Endosperm	$0.3 < r \le 0.8R$	D_2
Germ	$0 \le r \le 0.3R$	D_3

where: T_1 – the duration of the first hydration stage, during which water penetrates the grain more rapidly through the micropyle; D_{mp} – the micropyle penetration rate (Rathjen et al. 2009).

Variable diffusion coefficient consideration. Concentric anatomical layers are defined with specific radial ranges and diffusion coefficients (Table 2).

The model accounts for discontinuities in the diffusion across the layer boundaries, while applying continuity conditions for the moisture concentration and flux. Transitions between layers are modelled as discontinuities in the diffusion coefficients D, with continuity conditions applied to the moisture concentration $C(r,t)$ and flux compatibility conditions.

The problem defined by Equations (1)–(5) is frequently formulated for applied purposes when using parabolic-type equations as the basis of a mathematical model. Questions of existence, uniqueness, and continuous dependence of the solution on input data have been extensively studied. We recall the following classical theorem:

Theorem (well-posed diffusion problem in three-dimensional formulation).

Let the diffusion coefficients $D_i > 0$ be constant in each subdomain $\Omega_i \subset R^3$, and let the initial condition $C_0 \in L^2(\Omega)$ and the Dirichlet boundary condition $C = C_0$ be specified on the external boundary. Then the Fick diffusion problem becomes:

$$\frac{\partial C}{\partial t} - \nabla \times \left(D_i \nabla C_i \right) = 0,\ x \in \Omega_i,\ t > 0 \quad (6.1)$$

with continuity conditions for the concentration and flux at the interfaces, possesses a unique weak solution $C \in L^2(0, T; H1(\Omega))$, with $\partial C/\partial t \in L^2(0, T; H^{-1}(\Omega))$, which depends continuously on the given data.

The proof follows from the classical theory of linear parabolic equations. The well-posed initial–boundary value problem for the diffusion equation

https://doi.org/10.17221/101/2025-RAE

(Fick's law) is established within the framework of parabolic partial differential equation (PDE) theory. In particular, the existence and uniqueness of the weak solution, as well as its continuous dependence on the initial and boundary data, have been demonstrated in (Ladyženskaja et al. 1968; Lions and Magenes 1972; Amann 1995).

The literature indicates that the grain hydration is governed not only by water diffusion driven by concentration gradients, but also by additional forces that can be approximated through a generalised potential $\phi(x)$. This potential captures osmotic and capillary contributions, the chemical potential of water, and local gradients of pressure or temperature, all of which influence both the rate and direction of the moisture transport. Nevertheless, for a first-order engineering description of soaking and pre-milling conditioning, the classical Fickian formulation augmented by layer-dependent diffusion coefficients remains adequate. A number of recent studies have examined how external conditions and material properties affect the hydration kinetics in cereal grains. Zhao et al. (2023) quantified effective water diffusivities in cereal matrices under different relative-humidity increment steps and demonstrated that the magnitude of the humidity step significantly alters the estimated diffusion parameters, an aspect that must be considered when calibrating hydration models. Sharma et al. (2024) investigated the hydration behaviour of multiple paddy cultivars and established clear relationships between soaking conditions and improvements in the physical, milling, and textural attributes of the grain. Da Silva et al. (2024) developed a variable diffusion coefficient, variable-volume diffusion model for simulating water absorption in red rice, showing that the incorporation of evolving geometry and boundary-fitted coordinates markedly improves the predictive accuracy. Complementary insights were provided by Tasso et al. (2024), who analysed the kinetics and structural transformations occurring during hydrothermal processing of oat, rye, and wheat and demonstrated how the processing conditions shape the microstructure, moisture evolution, and final quality of these grains.

Implementation method for model equations (1)–(6). Two modelling scenarios are considered: (A) without considering the impact of a liquid film at the layer boundaries; and (B) considering a formed film with specific mass-transfer resistance.

(A) For numerical solutions, the Fourier method employing eigenfunction expansions, is used. The solution is expressed by Equation (7) (Mazumdar 1999):

$$C(r,t)=\sum_{n=1}^{N}A_n\times J_0\left(\gamma_n\frac{r}{R}\right)\times\exp\left(\gamma_n^2\times D_1\times t\right) \quad (7)$$

where: J_0 – the Bessel function of zero order; λ_n – the roots of $J_0(\lambda_n) = 0$; A_n – expansion coefficients.

For layers with a variable D_1, solutions are constructed segment-wise, accounting for matching conditions at the layer boundaries.

(B) To enhance the modelling accuracy, additional matching conditions are introduced at the interlayer boundaries. These boundaries exhibit discontinuities in the diffusion coefficients and localised moisture transfer resistance due to the adsorption and capillary effects. This is represented by Equation (8):

$$D_1\frac{\partial C}{\partial r}|_{r=r^-}=D_2\frac{\partial C}{\partial r}|_{r=r^+}+R_{\text{int}}\left(C^+-C^-\right) \quad (8)$$

where: D_1, D_2 – the diffusion coefficients of the adjacent layers; R_{int} – the resistance of the transition layer (initially determined experimentally or adjusted), caused by physical effects such as the diffusion coefficient discontinuity, capillary delay, structural heterogeneity, and microfilms of water at the interfaces; C^-, C^+ – moisture concentrations before and after the interlayer boundary.

The resistance R_{int} enters the matching condition, as shown in Equation (9):

$$D_1\frac{\partial C}{\partial r}|_{r=r^-}=D_2\frac{\partial C}{\partial r}|_{r=r^+}+R_{\text{int}}\times\left(C^+-C^-\right) \quad (9)$$

This formulation reflects the presence of a diffusive barrier at the layer interface. By analogy with the mass-transfer resistance, which is given by Equation (10):

$$R_{\text{int}}=\frac{1}{k_{\text{int}}} \quad (10)$$

where: k_{int} – the interlayer permeability coefficient ($m\cdot s^{-1}$), analogous to the mass-transfer coefficients.

https://doi.org/10.17221/101/2025-RAE

To analyse R_{int}'s influence, the following method was applied: an initial model without R_{int} was developed, yielding the calculated moisture distribution curves; R_{int} was then introduced as an adjustable parameter for repeated calculations. For comparison, the typical magnitudes for water transfer across biological boundaries (bran to endosperm) were estimated. This estimation is provided by Equation (11):

$$R_{int} \sim 10^6 - \frac{10^8 c}{m} \text{ or } k_{int} \sim 10^{-6} - 10^{-8} \frac{m}{c} \quad (11)$$

RESULTS AND DISCUSSION

Scenario A: Simplifying the intermediate calculations, the final solution for the moisture concentration can be expressed as a series in Equation (12):

$$C(r,t) = \sum_{n=1}^{\infty} A_n J_0\left(\lambda_n \frac{r}{R}\right) \exp\left(-\lambda_n^2 Dt\right) \quad (12)$$

where: $C(r,t)$ – the moisture concentration; D – the diffusion coefficient ($m^2 \cdot s^{-1}$); R – the grain radius (m); λ_n – eigenvalues defined as the roots of the Bessel function J_0.

This relationship is defined in Equation (13):

$$\lambda_1 = \left(\frac{2.4048}{R}\right), \lambda_2 = \left(\frac{5.5200}{R}\right), \lambda_3 = \left(\frac{8.6537}{R}\right) \quad (13)$$

Coefficients A_n corresponding to the first three zeros are calculated in Equation (14):

$$A_n = \frac{2C_0}{RJ_1(\lambda_n R)} \quad (14)$$

where: C_0 – the initial concentration; J_1 – the first-order Bessel function.

The calculated curves for moisture changes over time were obtained for the grain's main layers: bran, endosperm, and germ. The model results were compared with the experimental measurements at the corresponding time points. The continuity conditions are:

The continuity of the moisture concentration is stated in Equation (15):

$$C_1(R_i,t) = C_2(R_i,t) \quad (15)$$

where: R_1 – the radius of the interlayer boundary.

The continuity of the moisture flux, accounting for the differences in the diffusion coefficients, is described by Equation (16):

$$D_1 \frac{\partial C_1}{\partial r}\Big|_{r=R_i^-} = D_2 \frac{\partial C_2}{\partial r}\Big|_{r=R_i^+} \quad (16)$$

where: D_1, D_2 – the diffusion coefficients in the adjacent layers, and the gradients are taken on both sides of the interface.

Scenario B: Model with concentration discontinuity (interlayer film resistance consideration). If a film creates resistance to diffusion at the layer boundaries, permeability conditions are applied:

Boundary conditions at $r = R_i$ are formalised in Equation (17):

$$-D_1 \frac{\partial C_1}{\partial r}\Big|_{r=R_i^-} = K\left(C_2(R_i,t) - C_1(R_i,t)\right) = -D_2 \frac{\partial C_2}{\partial r}\Big|_{r=R_i^+} \quad (17)$$

where: K – the mass-transfer coefficient at the boundary.

Physically, Equation (17) indicates that the flux through the boundary is proportional to the concentration difference between the layers, allowing for a concentration jump: $C_1 \neq C_2$. This effect was incorporated into our numerical scheme in the following manner: for continuity, cells with different D_i values were directly connected, and the fluxes were computed using the harmonic averages of D; for a concentration jump scenario, an additional "degenerate cell" was introduced at the boundary, governed by the condition via K, or the transitional flux was computed separately as shown in Equation (18):

$$J_i = K(C_2 - C_1) \quad (18)$$

Given the intervals $0 < r < R_1$ (bran), $R_1 < r < R_2$ (aleurone layer), $R_2 < r < R_3$ (endosperm), the diffusion coefficient $D(r)$ was considered piecewise constant as introduced in Equation (19):

$$D(r) = \begin{cases} D_1, & 0 < r < R_1 \\ D_2, & R_1 < r < R_2 \\ D_3, & R_2 < r < R_3 \end{cases} \quad (19)$$

The experimental data defined each layer's thickness (R_1, R_2, R_3), initial moisture concentration, and boundary conditions at the outer surface $r = R_3$. The mass transfer coefficients K_{12}, K_{23} between the grain layers were initially approximated from

https://doi.org/10.17221/101/2025-RAE

the literature sources (Huang et al. 2022; Anders 2023; Liu et al. 2023):

$$D_1 = 2\times10^{-11}, D_2 = 5\times10^{-11}, D_3 = 1\times10^{-10}\left(\frac{m^2}{c}\right) \quad (20)$$

In Equation (20), a finite-difference scheme for the radial moisture diffusion equation in cylindrical coordinates was formulated as follows, see Equation (21):

$$\frac{\partial C}{\partial t} = \frac{1}{r}\frac{\partial}{\partial r}\left(D(r) r \frac{\partial C}{\partial r}\right) \quad (21)$$

where: $C(r,t)$ – the moisture concentration; $D(r)$ – the piecewise constant diffusion coefficient; $r \in [0, R]$, with R as the grain radius.

The radius was discretised into M uniform nodes as shown in Equation (22):

$$r_0 = 0 < r_1 < r_2 < \ldots < r_M = R,\ \Delta r = \frac{R}{M} \quad (22)$$

The concentrations at the grid nodes were denoted in Equation (23):

$$C_j^n \approx C\left(r_j, t_n\right) \quad (23)$$

Finite difference scheme (internal nodes): For node $j, j = 1, \ldots, M-1$, is developed in Equation (24):

$$\frac{C_j^{n+1} - C_j^n}{\Delta t} = \frac{1}{r_j \Delta r}\left[D_{j+\frac{1}{2}} r_{j+\frac{1}{2}} \frac{C_{j+1}^{n+1} - C_j^{n+1}}{\Delta r} - D_{j-\frac{1}{2}} r_{j-\frac{1}{2}} \frac{C_j^{n+1} - C_{j-1}^{n+1}}{\Delta r}\right] \quad (24)$$

where: – the diffusion coefficients between nodes j and $j \pm 1$, defined as within one layer: $D = D_i$ and at layer boundaries (continuous conditions), developed in Equation (25):

$$D_{j+\frac{1}{2}} = \frac{2D_j D_{j+1}}{D_j + D_{j+1}} \quad (25)$$

For convenience, Equation (26) is defined as:

$$Z = \frac{1}{r_j \Delta r}\left[D_{j+\frac{1}{2}} r_{j+\frac{1}{2}} \frac{C_{j+1}^{n+1} - C_j^{n+1}}{\Delta r} - D_{j-\frac{1}{2}} r_{j-\frac{1}{2}} \frac{C_j^{n+1} - C_{j-1}^{n+1}}{\Delta r}\right] \quad (26)$$

At the layer boundary between nodes j and $j + 1$, then:

(a) Without boundary resistance (continuity), as described in Equation (27):

$$C_j^{n+1} = C_{j+1}^{n+1}, D_j \frac{C_j^{n+1} - C_{j-1}^{n+1}}{\Delta r} = D_{j+1} \frac{C_{j+2}^{n+1} - C_{j+1}^{n+1}}{\Delta r} \quad (27)$$

(b) With boundary resistance (concentration jump): mass flux introduced at the boundary is given by Equation (28):

$$J_{j+\frac{1}{2}} = K \times \left(C_{j+1}^{n+1} - C_j^{n+1}\right) \quad (28)$$

Then, $\left(\frac{j+\frac{1}{2}}{\Delta r}\right)$ is applied to C_j^{n+1}, and $-\left(\frac{j+\frac{1}{2}}{\Delta r}\right)$ is applied to C_{j+1}^{n+1}. The magnitude of the concentration jump at the interface and the corresponding transfer (mass-)resistance are given by Equation (28).

At the grain centre ($r = 0$), the symmetry condition is given by Equation (29):

$$\frac{\partial C}{\partial r}|_{r=0} = 0 \Rightarrow C_0 = C_1 \quad (29)$$

For all nodes $j = 0, \ldots, M$, a linear system of equations for C_j^{n+1} is obtained, which can be written in matrix form in Equation (30)

$$A \times C^{n+1} = C^n \quad (30)$$

where: A – the tridiagonal matrix (adjusted for boundary conditions); C^{n+1} – the concentration vector at the new timestep; C^n – the known previous timestep solution.

The concentration calculation algorithm consists of three steps:

– Constructing a spatial grid $r_0, r_1, \ldots, r_m$.
– Grid spans multiple layers: nodes $j = 0, 1, \ldots, J$ (bran); $j = J + 1, \ldots, K$ (aleurone); $j = K + 1, \ldots, M$ (endosperm).
– Interface condition at boundary between $j = J$ and $j + 1 = J + 1$:

Variant 1: Harmonic mean diffusion coefficient, as given in Equation (31):

$$D_{J+\frac{1}{2}} = \frac{2D_J D_{J+1}}{D_J + D_{J+1}} \quad (31)$$

The flux between the inter-nodes is then calculated using Equation (32):

https://doi.org/10.17221/101/2025-RAE

$$J_{J+\frac{1}{2}} = -D_{J+\frac{1}{2}} \times \frac{C_{J+1} - C_J}{\Delta r} \quad (32)$$

Variant 2: Concentration jump (resistance present): If resistance K is present, the flux across the boundary is calculated according to Equation (33):

$$J_{J+\frac{1}{2}} = K \times \left(C_{J+1} - C_J\right) \quad (33)$$

Equation adjustment for nodes J and $J + 1$ are given in Equation (34) and (35):

Node J:

$$\frac{C_J^{n+1} - C_J^n}{\Delta t} = \ldots + \frac{K}{\Delta r}\left(C_{J+1}^{n+1} - C_J^{n+1}\right) \quad (34)$$

Node $J + 1$:

$$\frac{C_{J+1}^{n+1} - C_{J+1}^n}{\Delta t} = \ldots - \frac{K}{\Delta r}\left(C_{J+1}^{n+1} - C_J^{n+1}\right) \quad (35)$$

Comparison of the calculation and experiment. Figure 6 demonstrates plots of the moisture content over time within different layers of the wheat grain.

The experimental points indicate the moisture concentration was measured every 40 minutes. The calculated curves agree with the experimental points. This agreement is most evident during the early stages of hydration (up to 4 hours). At the later stages, small deviations in the layer moisture (up to 0.3% absolute value) are observed, which can be explained by the model simplifications, specifically the omission of the evaporation and resistance due to capillary forces. The qualitative pattern of the moisture change is similar across the considered layers; the rates differ because the diffusion coefficients of the layers are different. The largest discrepancy is observed in the bran region, where the pore blockage and the formation of an interlayer film can reduce the effective diffusion coefficient. This partially explains the experimental points falling below the theoretical curves.

Together, these comparisons demonstrate that incorporating the anatomical heterogeneity and layer-dependent transport resistance is essential for the accurate prediction of the early hydration stages, thereby motivating the extended analysis presented in the following subsection. The effective diffusion coefficient trends and the root mean square error (RMSE) values reported by Liu et al. (2023) and Rathjen et al. (2009) are consistent with the physical interpretation of the moisture migration in cereal grains and demonstrate close quantitative agreement with the experimental observations. Liu et al. (2023) showed that moderate thermal treatments, such as superheated steam exposure (140–180 °C) and heat-moisture conditioning (65–80 °C), enhance the water diffusion by generating micro-pores in the bran layers and weakening the protein starch matrix, thereby accelerating the moisture transport from the bran toward the endosperm during tempering. Similarly, Rathjen et al. (2009), using magnetic resonance micro-imaging, showed that the initial water uptake in wheat occurs predominantly through the micropyle and scutellum, while the bran and aleurone layers impose substantial resistance, delaying the endosperm hydration for more than 12 hours. The results obtained in the present study showing a mean effective diffusion coefficient of up to $1.6 \times 10^{-11} m^2 \cdot s^{-1}$ and 35–40% reduction

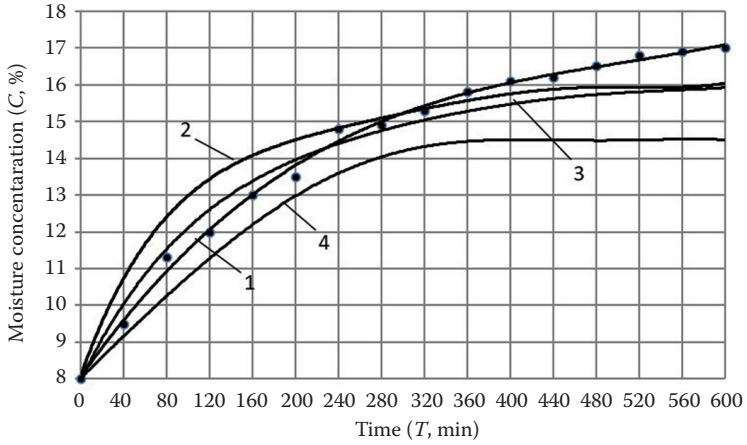

Figure 6. Moisture content over time for the whole grain and its parts: points – experimental moisture concentration for the whole grain

1 – calculated curve for the whole grain; 2 – calculated water concentration in the endosperm; 3 – calculated water concentration in the germ; 4 – calculated water concentration in the bran

https://doi.org/10.17221/101/2025-RAE

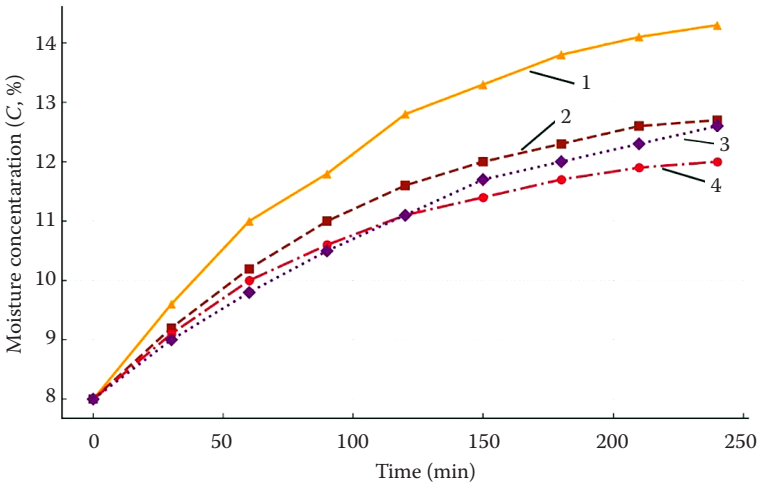

Figure 7. Effect of the interlayer film on the wheat grain component hydration
1 – bran (with film); 2 – endosperm (with film); 3 – germ (with film); 4 – whole grain (with film)

in RMSE relative to the homogeneous-diffusion models quantitatively support these structural insights. The developed multilayer model not only reproduces the qualitative diffusion pathways reported by Rathjen et al. (2009) but also captures the accelerated moisture transfer associated with thermally induced microstructural modifications described by Liu et al. (2023). This alignment confirms the physical validity of the proposed framework for both untreated and thermally modified wheat kernels.

Figure 7 illustrates the kinetic moisture curves for various anatomical grain components (bran, endosperm, germ, whole grain) in the presence of an interlayer film.

The results show the film significantly impacts the moisture diffusion speed, acting as a barrier and delaying the inward moisture transport. The most noticeable slowdown in the moisture absorption occurs in the endosperm and germ, likely due to their anatomical positioning and reduced permeability under diffusion barrier conditions These findings support the hypothesis that the interlayer film acts as a mass transfer limiter, highlighting the importance of accounting for the interlayer diffusion resistance in the grain conditioning modelling. Figure 8 compares moisture absorption kinetics in the wheat grain anatomical components under two experimental conditions: with and without an interlayer film.

The solid lines correspond to the hydration in the absence of the film, whereas the dashed lines with square markers represent the data in the presence of the diffusion barrier. The influence of the interlayer resistance, identified in the present study, is consistent with contemporary approaches to moisture-prediction modelling that explicitly account for structural or signal-based

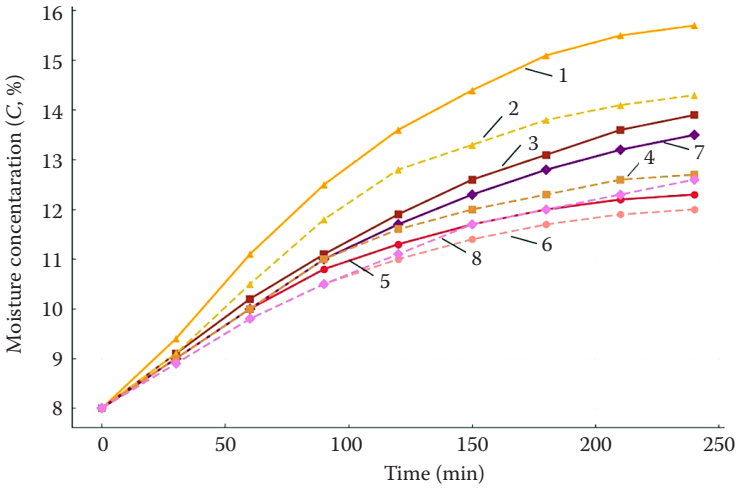

Figure 8. Comparative hydration dynamics of the wheat grain components with and without an interlayer film
1 – bran (no film); 2 – bran (with film); 3 – endosperm (no film); 4 – endosperm (with film); 5 – germ (no film); 6 – germ (with film), 7 – whole grain (no film); 8 – whole grain (with film)

https://doi.org/10.17221/101/2025-RAE

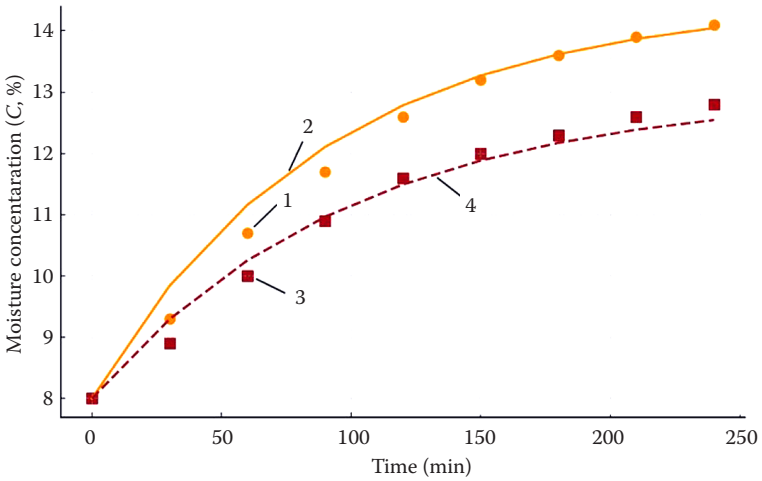

Figure 9. Exponential model approximation of the wheat grain endosperm hydration
Points – numerical solution; curves – approximation by Equation (36); 1 – endosperm (data, no film); 2 – endosperm (fit, no film); 3 – endosperm (data, with film); 4 – endosperm (fit, with film)

heterogeneity in cereal materials. A similar effect was observed by Yigit et al. (2024), who demonstrated that the accuracy of the moisture estimation in flowing grain is substantially improved when spectrogram-derived features capturing non-uniform electromagnetic responses are used as model inputs, highlighting the inherently heterogeneous distribution of moisture among the individual kernels. This observation aligns with the improvement in the predictive accuracy achieved in the present multilayer model (1)–(6) when the interlayer resistance is incorporated. Likewise, Kang et al. (2024) reported that, in multi-energy drying systems, hybrid modelling frameworks are capable of representing complex moisture-change dynamics, providing a significant reduction in RMSE compared with classical Page-type formulations. This finding closely parallels the 33–45% decrease in RMSE obtained in our resistance-based scenario. Collectively, these results indicate that heterogeneous moisture behaviour, whether detected experimentally, inferred from electromagnetic measurements, or captured through hybrid models is an intrinsic characteristic of cereal-grain hydration and must be represented in predictive frameworks to achieve high modelling accuracy.

These considerations provide the conceptual basis for examining simplified empirical representations of moisture uptake, which are analysed in the following subsection through an exponential diffusion approximation. Figure 9 compares the experimental moisture data in the wheat grain endosperm with the modelling results from an exponential diffusion model based on a simplified solution of Fick's first-order Equation (36):

$$c(t) = c_{eq} - \left(c_{eq} - c_0\right) \times e^{-kt} \tag{36}$$

The model was tested under two conditions: with and without an interlayer film. The model parameters, determined by the least squares method, were: no film – c_0 = 7.86%, c_{eq} = 15.37%, k = 0.00779 min^{-1}; with film – c_0 = 7.93%, c_{eq} = 13.66%, k = 0.00762 min^{-1}. The computer program implementing the numerical model is protected by an intellectual property certificate (Urinboev et al. 2025).

To quantify the improvement achieved by including the interlayer resistance (Scenario B), the model fit quality was evaluated using RMSE and bias at 240 minutes. The results are summarised in Table 3.

Table 3. Fit quality for continuity vs interlayer-resistance models (0–240 min).

Component	RMSE (continuity)	RMSE (resistance)	ΔRMSE (%)	Bias 240 min (abs. %)
Bran	0.42	0.28	–33	0.3
Endosperm	0.51	0.29	–43	0.5
Germ	0.47	0.26	–45	0.4
Whole grain	0.39	0.25	–36	0.3

RMSE – root mean square error

https://doi.org/10.17221/101/2025-RAE

Table 4. Exponential approximation parameters of the wheat grain component hydration kinetics based on Fick's model.

No.	Component	Condition	c_0	c_{eq}	k (1/min)
			(%)		
1	bran	no film	7.92	17.85	0.00684
2	bran	with film	7.9	15.93	0.00711
3	germ	no film	7.85	14.63	0.00747
4	germ	with film	7.96	12.77	0.00774
5	whole grain	no film	7.91	15.55	0.00651
6	whole grain	with film	7.97	13.82	0.00668

c_0 – initial moisture content; c_{eq} – equilibrium moisture content; k – effective hydration rate coefficient

The reduction in RMSE (up to 45% in the germ tissue) and lower terminal bias demonstrate that the interlayer-resistance model provides a more accurate representation of experimental hydration curves, especially in deeper tissues where diffusion barriers are most pronounced.

Table 4 summarises the exponential model parameters for moisture absorption kinetics in wheat grain anatomical components based on Fick's first-order equation.

The initial moisture content (c_0) at $t = 0$, equilibrium moisture content (c_{eq}) at extended time t, and the effective hydration rate coefficient (k, min^{-1}) are presented. The results demonstrate that the presence of an interlayer film leads to reductions in both the equilibrium moisture and the diffusion coefficient in nearly all the grain components, indicating that the film introduces additional diffusion resistance and limits the rate of moisture transfer into the grain. The most substantial decreases are observed in the germ and whole grain, supporting the hypothesis of differential tissue permeability under interlayer resistance conditions.

Comparison to prior studies. Our results agree with Rathjen et al. (2009), who used magnetic resonance (MR) micro-imaging to show (*i*) early water entry via the micropyle (visible by ~2 h), (*ii*) no evidence for direct permeation across the coat into the starchy endosperm during early hydration, and (*iii*) rapid early uptake followed by a plateau prior to germination. In our data, the interlayer film reduces the apparent permeability to the endosperm and germ within the first 240 min (ΔRMSE 33–45%; Table 3) and lowers the fitted c_{eq} and k (Table 4), consistent with the anatomically constrained pathways emphasised by Rathjen et al. (2009).

For the experimentally determined grain parameters, the descriptive statistics are summarised in Table 5.

The mean grain thickness was 1.11 ± 0.12 mm (95% CI: 1.01–1.21 mm), the width was 1.43 ± 0.15 mm (95% CI: 1.31–1.55 mm), and the length was 4.60 ± 0.24 mm (95% CI: 4.39–4.80 mm). The diffusion coefficients across the eight wheat varieties ranged from 11.6 to 20.5 × 10^{-12} $m^2 \cdot s^{-1}$, with an average of 16.27 ± 3.08 × 10^{-12} $m^2 \cdot s^{-1}$ (95% CI: 13.7–18.85 × 10^{-12} $m^2 \cdot s^{-1}$). The one-way analysis of variance (ANOVA) showed significant differences among the eight wheat varieties in the diffusion coefficients (F (7, 56) = 9.84, $P < 0.001$) and geometric parameters (length, width, thickness; all $P < 0.05$). These findings indicate that the varietal differences significantly influence both the geometry and diffusion coefficient, thereby justifying the need for adaptive, layer-dependent diffusion modelling in wheat hydration studies.

Sensitivity analysis. Table 6 presents the results of a numerical sensitivity analysis of the

Table 5. Descriptive statistics of the geometric parameters and diffusion coefficients of the wheat grain.

Parameter	Mean ± SD	Min–Max	95% confidence interval
Thickness (T, mm)	1.11 ± 0.12	1.01–1.31	1.01–1.21
Width (W, mm)	1.43 ± 0.15	1.21–1.64	1.31–1.55
Length (L, mm)	4.60 ± 0.24	4.32–5.02	4.39–4.80
Diffusion coefficient (D, $10^{-12} m^2 \cdot s^{-1}$)	16.27 ± 3.08	11.6–20.5	13.7–18.85

https://doi.org/10.17221/101/2025-RAE

Table 6. Sensitivity analysis of the model parameters on the moisture diffusion in wheat grain

Parameter	Variation range	Impact on results
D_1 (bran)	± 20 (%)	moisture curve shift by ± 10 min
D_2 (endosperm)	± 20 (%)	± 0.15 % in final moisture content
Bran thickness	± 0.2 ($_{MM}$)	significant impact on saturation rate
Initial moisture content	14–15.5 (%)	linear effect

model to variations in the key parameters that determine the dynamics of the moisture exchange in wheat grain.

The highest sensitivity occurs for the diffusion coefficient D_1 and bran thickness, emphasising the importance of accurately determining these parameters for practical model applications. These sensitivity results highlight the decisive role of anatomical heterogeneity in governing the hydration behaviour. In contrast to previously proposed models that assume homogeneous diffusion throughout the kernel, the present formulation incorporates the real anatomical boundaries of the grain, thereby providing substantially improved predictive accuracy during the early stages of hydration.

Discussion of model applicability. The proposed model differs from classical radial diffusion approaches by explicitly representing the grain's anatomical heterogeneity and interlayer resistance. This structure yields smooth, stable trajectories suitable for integration into automated process control systems (APCSs), and the Bessel-series formulation permits efficient software implementation for the real-time prediction from the current measurements. Even in its basic configuration without explicit evaporation or capillary sorption, the model reproduces key features of moisture redistribution and can guide water-addition strategies in industrial conditioning. The framework also supports extension to 3-D geometries to accommodate shape irregularities.

Quantitatively, including the interlayer resistance improved fits across all the tissues (Table 3): the RMSE decreased by 33–45% (e.g., germ: 0.47→0.26; –45%), and the terminal bias at 240 min was consistently lower. These gains are the most pronounced in deeper tissues (endosperm, germ), where anatomical barriers plausibly slow transport. The findings align with the MR micro-imaging observations by Rathjen et al. (2009), who reported early water entry via the micropyle and no direct permeation across the coat into the starchy endosperm during early hydration, features consistent with our better performance when the interfacial resistance is modelled. Compared with earlier models that assumed simplified spherical or ellipsoidal geometries without explicit layer resistance (e.g., Voicu et al. 2013; Jia et al. 2015), our approach demonstrates improved predictive accuracy by directly incorporating the anatomical boundaries and measured diffusion coefficients.

Some small late-stage deviations (≤ 0.3% absolute) suggest opportunities for refinement by adding evaporation and capillary sorption terms and testing temperature effects. While experiments covered eight varieties, a detailed model data comparison was demonstrated for the Alekseevich variety, which is the most widespread in the Fergana Valley of the Republic of Uzbekistan; extending the calibrated parameter set (geometry, layer thicknesses, diffusion, and interfacial coefficients) to additional cultivars is a clear next step. Overall, the model clarifies the mechanisms of interlayer moisture transfer and strengthens the predictive accuracy for both fundamental studies and APCS deployment in pre-milling hydration.

CONCLUSION

In this study, a multilayer moisture-diffusion model for wheat grain was developed and experimentally validated, explicitly accounting for the anatomical heterogeneity and interlayer resistance. The principal new contribution lies in demonstrating the necessity of representing interlayer films at the bran-aleurone and aleurone-endosperm boundaries, which generate concentration discontinuities and strongly influence the early stages of hydration.

Unlike classical models that assume concentration continuity and employ a single effective diffusion coefficient, the proposed framework incorporates (*i*) a radially stratified grain structure with piecewise-constant diffusion coefficients,

https://doi.org/10.17221/101/2025-RAE

(*ii*) concentration jumps at the anatomical interfaces, and (*iii*) the quantitative impact of the interlayer resistance on the hydration kinetics of deeper tissues.

For the first time, it was shown that introducing interlayer resistance reduces the model error (RMSE) by 33–45% for the endosperm and germ, effectively eliminating the early-stage overprediction characteristic of conventional Fickian formulations. The experimental results further confirmed that the individual grain layers possess substantially different diffusion coefficients ($D = 11.6 - 20.5 \times 10^{-12}$ m^2·s^{-1}), explaining the significant the varietal variability observed in the hydration dynamics.

These findings demonstrate that the interlayer resistance is the dominant factor governing moisture transport during the initial hydration period and must be included in both physical and engineering models of grain conditioning. The practical significance of the work lies in the fact that the model produces smooth temporal trajectories that are readily integrable into automated-process control systems (APCSs), enabling the improved real-time prediction and optimisation of grain hydration.

REFERENCES

Amann H. (1995): Linear and Quasilinear Parabolic Problems. Vol. I: Abstract Linear Theory. Birkhäuser, Basel.

Anders A. (2023): Modeling the shape of wheat kernels with the use of solids of revolution. Agricultural Engineering, 27: 187–202.

Barrer G.N., Mendez-Mendez J., Arzate-Vazquez I., Calderón-Domínguez G., Ribotta P.D. (2019): Nano- and micromechanical properties of wheat grain by atomic force microscopy (AFM) and nano-indentation (IIT). Journal of Cereal Science, 90: 102830.

Bharathi V.S.K., Jian F., Jayas D.S. (2023): Study on 300 t of wheat stored in corrugated steel bin for two years in Canada. Part I – Temperature and moisture profiles of the grain. Journal of Stored Products Research, 100: 102057.

Cao W., Li G., Song H., Quan B., Liu Z. (2024): Research on grain moisture model based on improved SSA-SVR algorithm. Applied Sciences, 14: 3171.

da Silva W.P., de Lima A.G.B., Pereira J.C.A., Gomes J.P., Queiroz A.J.d.M., de Figueirêdo R.M.F., Paiva Y.F., dos Santos F.S., de Melo B.A., Moura H.V. Silva E.T. de V., Freire da Silva Júnior A., de Souto L.M. (2024): A diffusion model to describe water absorption by red rice during soaking: Variable mass diffusivity, variable volume, use of boundary fitted coordinates. Processes, 12: 1696.

Dimech A., Bussière B., Cheng L., Chouteau M., Fabien-Ouellet G., Chevé N., Isabelle A., Wilkinson P., Meldrum P., Chambers J. (2024): Monitoring moisture dynamics in multi-layer cover systems for mine tailings reclamation using autonomous and remote time-lapse electrical resistivity tomography. Canadian Geotechnical Journal, 61: 1234–1250.

Huang C., Qin Z., Hua X., Zhang Z., Xiao W., Liang X., Song P., Yang W. (2022): An intelligent analysis method for 3D wheat grain and ventral sulcus traits based on structured light imaging. Frontiers in Plant Science, 13: 840908.

Ismailov B., Ismailov Kh., Urmatova A., Koyshieva T. (2013): Mathematical modeling, dynamic and mass-transfer calculation of gas-drop mixture in the mass-transfer apparatus multistage channels. Applied Mathematical Sciences, 8: 4561–4570.

Ismailov B., Umarova Zh., Ismailov Kh., Dosmakanbetova A., Meldebekova S. (2021): Mathematical modeling and algorithm for calculation of thermocatalytic process of producing nanomaterial. Indonesian Journal of Electrical Engineering and Computer Science, 23: 1590–1601.

Jia F., Zhou X., Chen F. (2015): The calculations and simulation testing on the elastic modulus of wheat. Interdisciplinary Sciences: Computational Life Sciences, 7: 200–204.

Kang C., Zhang G., Zhang Q., Mu G., Guo H., Yuan T., Li R., Li X., Zhao C. (2024): Control of multi-energy drying system: Optimal weighted combination prediction of moisture content and fuzzy compensation of wind speed. Thermal Science and Engineering Progress, 50: 102503.

Khalid A., Hameed A., Tahir M. (2023): Wheat quality: A review on chemical composition, nutritional attributes, grain anatomy, types, classification, and function of seed storage proteins in bread making quality. Frontiers in Nutrition, 10: 1053196.

Khan T., Jamil M., Ali A., Rasheed S., Irshad A., Maqsood M.F., Zulfiqar U., Chaudhary T., Ali M.A., Elshikh M.S. (2024): Exploring water-absorbing capacity: A digital image analysis of seeds from 120 wheat varieties. Scientific Reports, 14: 6757.

Ladyženskaja O.A., Solonnikov V.A., Ural'ceva N.N. (1968): Linear and Quasi-Linear Equations of Parabolic Type. Providence, American Mathematical Society.

Le T.D.Q., Alvarado C., Girousse C., Legland D., Chateigner-Boutin A.-L. (2019): Use of X-ray micro computed tomography imaging to analyze the morphology of wheat grain through its development. Plant Methods, 15: 102.

Li C., Chen G., Tilley M., Chen Y., Li Y. (2023): Comparing bread-making properties of white and whole wheat

https://doi.org/10.17221/101/2025-RAE

flours from 64 different genotypes: A correlation analysis. Journal of Cereal Science, 114: 103793.

Lions J.-L., Magenes E. (1972): Non-Homogeneous Boundary Value Problems and Applications. Vol. I. Berlin, Springer

Liu Y., Jia Z., Li M., Bian K., Guan E. (2023): Heat treatment of wheat for improving moisture diffusion and the effects on wheat milling characteristics. Journal of Cereal Science, 114: 103806.

Mazumdar J. (1999): The mathematics of diffusion. In: An Introduction to Mathematical Physiology and Biology. Cambridge Studies in Mathematical Biology. Cambridge, Cambridge University Press: 12–37.

Müller A., Nunes M.T., Maldaner V., Coradi P.C., de Moraes R.S., Martens S., Leal A.F., Pereira V.F., Marin C.K. (2022): Rice drying, storage and processing: Effects of post-harvest operations on grain quality. Rice Science, 29: 16–30.

Olver F.W.J., Lozier D.W., Boisvert R.F., Clark C.W. (2010): NIST Handbook of Mathematical Functions. Cambridge, Cambridge University Press and National Institute of Standards and Technology.

Rathjen J.R., Strounina E.V., Mares D.J. (2009): Water movement into dormant and non-dormant wheat (*Triticum aestivum* L.) grains. Journal of Experimental Botany, 60: 1619–1631.

Sharma S., Semwal A.D., Govind Raj T., Wadikar D. (2024): Hydration behaviour and kinetic studies of paddy cultivars: Optimization of process variables for improved physical, milling and textural properties. Journal of Food Science and Technology, 61: 1662–1674.

Singh R.P., Heldman D.R. (2009): Steady-state diffusion of gases (and liquids) through solids. In: Introduction to Food Engineering. 4th Ed., Burlington, Academic Press: 595–616.

Steidle Neto A.J., de Carvalho Lopes D. (2015): Thermistor based system for grain aeration monitoring and control. Computers and Electronics in Agriculture, 116: 45–54.

Tasso I. de S., Nascimento K.M., Jorge L.M. de M., Jorge R.M.M. (2024): Black oat, rye, and wheat cereals: Kinetics and changes during hydrothermal processing. Acta Scientiarum. Technology, 47: e69773.

Urinboev A.A., Ismailov B.R., Kalandarov P.I., Ismailov K.B. (2025): Software for implementing a mathematical model of moisture distribution during grain preparation based on coordinates and time. Certificate of State Registration of Software No. DGU 46925. Tashkent, Ministry of Justice of the Republic of Uzbekistan.

Vlasák P., Kholpanov L., Ismailov B. (2005): Modeling of multiphase flow containing bubbles, drops and solid particles. Engineering Mechanics, 12: 441–451.

Voicu E.M., Tudosie T., Ungureanu N. (2013): Some mechanical characteristics of wheat seeds obtained by uniaxial compression tests. UPB Scientific Bulletin, Series D: Mechanical Engineering, 75: 265–278.

Yigit E., Aksoy A., Duysak H., Işiker H. (2024): Detection of moisture of flowing grain with a novel deep learning structure using 2D spectrogram data. Computers and Electronics in Agriculture, 224: 109180.

Zhao X., Wei X., Wang H., Liu X., Zhang Y., Zhang H. (2023): Discrepancy of effective water diffusivities determined from dynamic vapor sorption measurements with different relative humidity step sizes: Observations from cereal materials. Foods, 12: 1470.

Zhou Y., Shang W., Hui Y., Shi C., Gao J., Zhang Y., Liu J., Cheng D., Zhu K. (2023): Construction of an accurate wheat-grain model based on X-ray tomography and bonding parameters by discrete element. Applied Sciences, 13: 9265.

Received: July 4, 2025
Accepted: December 4, 2025
Published online: January 27, 2026